

Journal of Biomedical Optics

SPIEDigitalLibrary.org/jbo

Noninvasive imaging of the early effect of sodium iodate toxicity in a rat model of outer retina degeneration with spectral domain optical coherence tomography

Sepideh Hariri
Man Chun Tam
Donghyun Lee
Denise Hileeto
Alireza Akhlagh Moayed
Kostadinka Bizheva

Noninvasive imaging of the early effect of sodium iodate toxicity in a rat model of outer retina degeneration with spectral domain optical coherence tomography

Sepideh Hariri,^a Man Chun Tam,^a Donghyun Lee,^a Denise Hileeto,^b Alireza Akhlagh Moayed,^a and Kostadinka Bizheva^a

^aUniversity of Waterloo, Department of Physics and Astronomy, Waterloo, Ontario, Canada

^bUniversity of Waterloo, School of Optometry and Vision Science, Waterloo, Ontario, Canada

Abstract. An ultrahigh resolution spectral domain optical coherence tomography (SD-OCT) system is used to observe for the first time *in vivo* the early effect of sodium iodate (NaIO_3) toxicity on retinal morphology. Retinal degeneration is induced in rats via tail vein injection of NaIO_3 and structural changes in the outer retina are assessed longitudinally at baseline and 1, 2, 3, 6, 8, and 10 h, and 12 post drug administration with OCT, H&E histology, and IgG immunochemistry. Disruption of the structural integrity and changes in the optical reflectivity of the photoreceptor inner (IS) and outer segment (OS) layers are observed as early as 1 h post NaIO_3 injection. A new layer is observed in the OCT tomograms to form between the retinal pigmented epithelium and the photoreceptors OS a few hours post NaIO_3 injection. The dynamics and the low optical reflectivity of this layer, as well as cell swelling and disruption of the blood-retina barrier observed in the histological and immunohistochemistry cross-sections suggest that the layer corresponds to temporary fluid accumulation in the retina. Results from this study demonstrate the effectiveness of OCT technology for monitoring dynamic changes in the retinal morphology and provide better understanding of the early stages of outer retina degeneration induced by NaIO_3 toxicity. © 2013 Society of Photo-Optical Instrumentation Engineers (SPIE) [DOI: 10.1117/1.JBO.18.2.026017]

Keywords: optical coherence tomography; medical and biological imaging; ophthalmic optics and devices; retina degeneration; sodium iodate.

Paper 12591 received Sep. 6, 2012; revised manuscript received Dec. 20, 2012; accepted for publication Jan. 2, 2013; published online Feb. 7, 2013.

1 Introduction

Sodium iodate (NaIO_3) is a drug commonly used to induce outer retina degeneration in animal models, specifically in rodents. It is known for its toxic effect on the retinal pigment epithelium (PRE) cells¹ that leads to retinal pigmented epithelium (RPE) cell necrosis, followed by photoreceptor (PR) cell apoptosis.^{2,3} The effect of this drug on animal retinas has been studied using different methods such as histology and immunohistochemistry,¹⁻⁹ auto-fluorescence microscopy,¹ vitreous fluorophotometry,⁴ fundus photography, and fluorescent angiography.¹⁰ Although histology and immunohistochemistry provide accurate and subcellular level resolution cross-sectional images of the retina, these methods are invasive (require animal euthanasia at each time point of a longitudinal study) and are prone to artifacts associated with the sample preparation. Fundus photography and fluorescent angiography allow for non- or minimally invasive *in vivo* imaging of the retinal surface and blood perfusion; however, they cannot provide high-resolution depth-resolved images of the layered retinal structure to evaluate the drug-induced morphological changes on individual retinal cell types.

Furthermore, a number of studies have been conducted in rodents to investigate the short-term effect of NaIO_3 on the

retina morphology within the first 24 h of drug administration. These studies utilized research methods such as histology, immunohistochemistry, electron microscopy^{2,5,9} and vitreous fluorophotometry.⁴ Defragmentation of RPE cell nuclei at ~ 2 h, disorganization of the rod outer segment discs⁹ at ~ 6 h, swelling of the PRE cytoplasmic organelles at ~ 6 h,⁵ decreased number of RPE cell nuclei at ~ 12 h,² and breakdown of the blood-retina barrier at ~ 24 h post drug administration⁴ were reported. Another study reported reduction in the adhesion between the RPE and the Bruch's membrane within the first 10 min, and between the RPE and the neuro-sensory retina about 2 h later.¹¹

Although ultrahigh resolution optical coherence tomography (UHR-OCT) has been used in the past to image *in vivo* healthy and diseased rodent retinas,¹²⁻¹⁷ until recently, this technology has not been used to image NaIO_3 treated rodent retinas. Recently, our research group demonstrated the effectiveness of high-speed UHR-OCT for noninvasive, *in vivo* three dimensional imaging of the morphological changes induced by NaIO_3 in the rat retina.¹⁸ In that study, rats were imaged on days 1, 3, and 7 and at months 1, 2, and 3 post drug injection, to evaluate the long term, acute effect of the drug toxicity.

In this study, we report for the first time, NaIO_3 induced changes in the retina morphology and optical properties, observed *in vivo* with UHR-OCT within the first 12 h of the drug administration. We show that the drug toxicity results in

Address all correspondence to: Kostadinka Bizheva, University of Waterloo, Department of Physics and Astronomy, 200 University Avenue West, Waterloo, Ontario, Canada N2L 3G1. Tel: (1) 519-888-4567x37517; E-mail: kbizheva@uwaterloo.ca

a temporary fluid accumulation at the OS/RPE boundary, commencing within the first 1 to 2 h post drug administration, that causes tearing of the OS from the RPE and precedes the apoptotic and necrotic processes in the photoreceptor and RPE cells previously reported in the literature.

2 Methods

2.1 UHR-OCT System

Briefly, the UHR-OCT system used in this study^{13,18} is based on a spectral domain OCT design and utilizes a fiber-optic Michelson interferometer, interfaced to a broad bandwidth superluminescent diode (SLD, Superlum, $\lambda_c = 1020$ nm, $\Delta\lambda = 108$ nm, and $P_{\text{out}} = 10$ mW). The interference signal is detected by a high efficiency spectrometer (P&P Optica) and a 1024 pixel linear array CCD camera (Sensors Unlimited, Goodrich) operating at 47 kHz readout rate. The system provided 3 μm axial resolution in the rat retina and ~ 99 dB sensitivity for 1.6 mW power of the imaging beam incident on the cornea. A custom imaging probe comprised of three achromat lenses (Linus, $f_1 = 10$ mm, Edmund Optics, $f_2 = 30$ mm and $f_3 = 60$ mm) and a pair of galvanometric scanners (Cambridge Technologies) was designed to project a 1-mm-diameter optical beam on the rat cornea and image the rat retina with $\sim 5 \mu\text{m}$ lateral resolution. Because typically rats are myopic or hyperopic, the imaging probe was designed to allow for adjustment of the distance between the focusing and imaging lenses of the probe, to generate a slightly convergent or slightly divergent imaging beams incident on the cornea, which can compensate for the animal's myopia or hyperopia.

2.2 Sodium Iodate Induced Toxicity Model in Rat Retina

Twenty eight 12- to 15-week-old female Long Evans rats were used for this study. All animal procedures were conducted in compliance with the University of Waterloo Animal Ethics Committee regulation and the ARVO statement for ethical use of animals in ophthalmic and vision research. Animals were anesthetized with isoflurane (2.5%) and pupils were dilated by administering 1 to 2 drops of tropicamide (Mydracyl, 1%). Outer retinal degeneration was induced by tail vein IV injections of 40 mg/kg of NaIO_3 . Artificial tears were administered frequently to keep the cornea hydrated and optically clear.

Eighteen animals were divided into two groups for the OCT imaging. In Group #1 ($n = 9$) six rats received NaIO_3 injections, and three control rats received equivalent amount of phosphate buffered saline (PBS) as vehicle thorough IV injections. The animals in Group #2 received either NaIO_3 ($n = 6$) or vehicle ($n = 3$), as well as 1 mL supplementary subcutaneous PBS injections at 1 and 3 h post NaIO_3 or vehicle administration, intended to decrease the severe adverse side effects of the drug. All animals from groups #1 and #2 were imaged with UHR-OCT at baseline and at 1, 2, 3, 6, 8, and 10 h, and 12 post NaIO_3 or vehicle injections and euthanized with CO_2 following that last imaging session. The imaging sessions adhered to a strict schedule, starting at ~ 9 a.m. and finishing at ~ 9 p.m. Volumetric UHR-OCT images were acquired from the same retinal location.

The remaining 10 animals were injected with both NaIO_3 and supplementary subcutaneous PBS, imaged and then

euthanized with CO_2 at different time points of the longitudinal study ($n = 2$ for each time point: baseline, 1, 3, 6, and 12 h of the study), and the eyes were harvested and preserved for histological analysis.

2.3 Image Acquisition and Data Processing

Three-dimensional (3-D) volumetric UHR-OCT tomograms were acquired from $\sim 2 \times 2$ mm area near the central retina, with the optic nerve head (ONH) located at the nasal-inferior edge of the imaged area. The 3-D image stacks were composed of 256 B-scans, while each B-scan was comprised of 1000 A-scans \times 512 pixels. Cross-sectional images of the rat retina were generated from the raw UHR-OCT data using a custom Matlab code (Mathworks). The structure of the optic nerve head and the branching blood vessels at the retinal surface were used as landmarks to assure consistency in imaging the same retinal location at all time points of the longitudinal study. Because of natural eye motion, successive B-scans in the 3-D data sets acquired at different time points of the longitudinal study from the same eye, were shifted or rotated with respect to each other. Therefore, we used a commercial 3-D rendering software to cross-correlate the B-scans and generate 3-D images of the rat retina. Subsequently, the 3-D images acquired at different time points of the study from the same animal were aligned with respect to each other to allow for overlap of the retinal blood vessels pattern at the ONH. An area of $\sim 1 \times 1$ mm (corresponding to a reduced 3-D stack of 128 B-scans of 500 A-scans each) was selected from the overlapping 3-D volumes for analysis of the thickness of reflectivity of the rat retinal layers. A semi-automatic segmentation algorithm developed in our research group¹⁹ was used to segment individual retinal layers from the UHR-OCT cross-sectional tomograms and to evaluate the retinal layer thickness and optical reflectivity. One 3-D stack was processed for each animal for each of time point of the longitudinal study. Because the segmentation algorithm is semi-automatic (requires initial input from the operator for processing each B-scan), only every tenth B-scan in the reduced 3-D stack was segmented and used for analysis. Data from the segmentation was used to determine the mean thickness of each segmented retinal layer, by averaging laterally over the width of the B-scan. The reflectivity of each layer was calculated by spatially averaging the OCT pixel intensity within the boundaries of the segmented layer. The intensity calculated for each layer was then normalized by the intensity of the inner plexiform layer (IPL), since previous studies have shown that NaIO_3 does not affect the IPL structure.

2.4 Statistical Analysis

Data acquired from all six NaIO_3 -injected and the three vehicle-injected (control) rats in each group of animals was analyzed to quantify the thickness and reflectivity changes observed in different retinal layers. For statistical analysis, one-way repeated measures ANOVA were used to determine the changes in the layer thickness and reflectivity as a function of time. Bonferroni-corrected multiple comparison tests were used as the post-hoc test. For all statistical tests, changes were considered significant at $p < 0.05$.

2.5 Histopathology

Two rats (four eyes) were imaged with UHR-OCT, euthanized at each time point (baseline, 1, 3, 6, and 12 h after NaIO₃ injection), and the eyes were enucleated and prepared for histopathological evaluation. The eyes were harvested from rats that have received the supplementary PBS injections. Consecutive sections of the entire retina were processed for microscopic analysis: after initial fixation in 10% neutral buffered formalin, the eyes were embedded in paraffin, serially sectioned in 5- μ m-thick sections, and stained with hematoxylin and eosin (H&E). For immunohistochemical analysis, one representative paraffin block was selected for each case, and stained using monoclonal IgG antibodies (dilution 1:50), utilizing the streptavidin-biotin peroxidase technique (Abcam, Cambridge, MA). Appropriate negative and positive controls were included. The histological slides were evaluated using bright field microscopy (Leica DM1000, Leica Microsystems Inc, Concord, ON). The histological cross-sections discussed in this manuscript were obtained from the same 1 \times 1 mm retinal area that was imaged with the spectral domain optical coherence tomography (SD-OCT) system.

3 Results

Figure 1(a) shows a representative cross-sectional UHR-OCT image of the healthy rat retina acquired at baseline, where all retinal layers are clearly visualized. Since this project focused on examining the early effect of NaIO₃ toxicity on the RPE and photoreceptor IS and OS, it was important to have a good understanding of the healthy rat retina morphology and specifically the outer retina, as visualized in the UHR-OCT images. Figure 1(b) shows a magnified view of the rat outer retina [area marked with the red rectangle in Fig. 1(a)], while Fig. 1(c) is an anatomically correct schematic of a photoreceptor and an RPE cell, similar to those found in retinal anatomy books. As observed in the UHR-OCT tomogram [Fig. 1(b)], the photoreceptor IS and OS layers consist of alternating low and high reflective bands, which starting from the top and following the analysis presented in a recent publication from Spaide and Curcio,²⁰ can be interpreted as: a very narrow and highly reflective external limiting membrane (ELM), composed from synapses of the Mueller cells; a low reflective band corresponding to the myoid, the upper section of the photoreceptors inner segment (IS1), which is filled with transparent cytoplasm and cellular organelles such as microfilaments,

Golgi apparatus and ribosomes that are less than 1 μ m in size, thus resulting in weak optical reflectivity; a highly reflective band corresponding to the ellipsoid, the lower part of the photoreceptors inner segment (IS2), which is filled with densely packed mitochondria with significantly higher refractive index (\sim 1.4)²¹ as compared to the surrounding cytoplasm (\sim 1.35)^{22,23}; a low reflective outer segment (OS1) consisting of double lipid membrane disks of fairly low refractive index; a highly reflective band (OS2), corresponding to the OS/RPE junction, filled with interspaced photoreceptor OS and highly reflective microvilli of the RPE cells, which contain large quantities of melanin granules of high optical refractive index (\sim 1.67)²⁴; the very thin and highly reflective line of the RPE layer, which contains large quantities of melanin. The detailed analysis of the rat outer retina morphology as visualized in the UHR-OCT images presented in Fig. 1 was used as a reference point to examine any structural changes in the photoreceptor and RPE layers caused by the NaIO₃ toxicity at different time points of the longitudinal study. UHR-OCT tomograms of the same appearance and quality were acquired from all rats at baseline and at all time points in the control animals.

Figure 2 shows representative UHR-OCT images from the rat retina acquired at all time points of the longitudinal study from one of the NaIO₃ injected rats. The typical layered structure of the normal healthy rat retina imaged at baseline is shown in Fig. 2(a). A magnified view (3 \times) of a section of the outer retina, marked with the red box in Fig. 2(a) is shown in Fig. 2(b), where the bright and dark bands of the PR layer are labeled following the method described in Fig. 1. Figure 2(c) shows a cross-sectional image of the same location in the retina, acquired 1 h post NaIO₃ injection. The previously clear band corresponding to the OS1 in Fig. 2(b), is now more optically scattering, and a new very low reflectivity layer (LRL) appears at the OS/RPE boundary. In the enlarged view [Fig. 2(d)], the RPE appears structurally intact, while the dark, band above it, most likely corresponds to loose ends of the photoreceptor OS that have been detached from the RPE layer. The end of the OS layer, located immediately above the LRL appears darker as compared with the baseline image, which suggest rearrangement of the loose photoreceptor OS, that can scatter light more, as compared to the case of the healthy rat retina, where the OS ends are neatly arranged in between the RPE microvilli and attached to the RPE.

Three hours after the NaIO₃ injection, the new LRL is no longer visible [Fig. 2(e)]. This is confirmed by the magnified view of the outer retina in Fig. 2(f), where the new LRL is

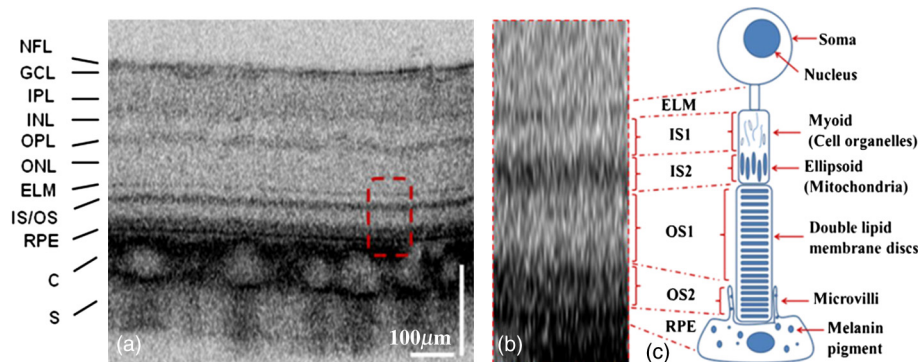


Fig. 1 A representative UHR-OCT tomogram acquired from a healthy rat retina with all retinal layers clearly visible and labeled (a) Magnified view of the photoreceptor and RPE layers (b) allows for direct correlation of the alternating low and highly reflective photoreceptor IS and OS bands to anatomical features of the rod photoreceptor cell in the schematic representation (c).

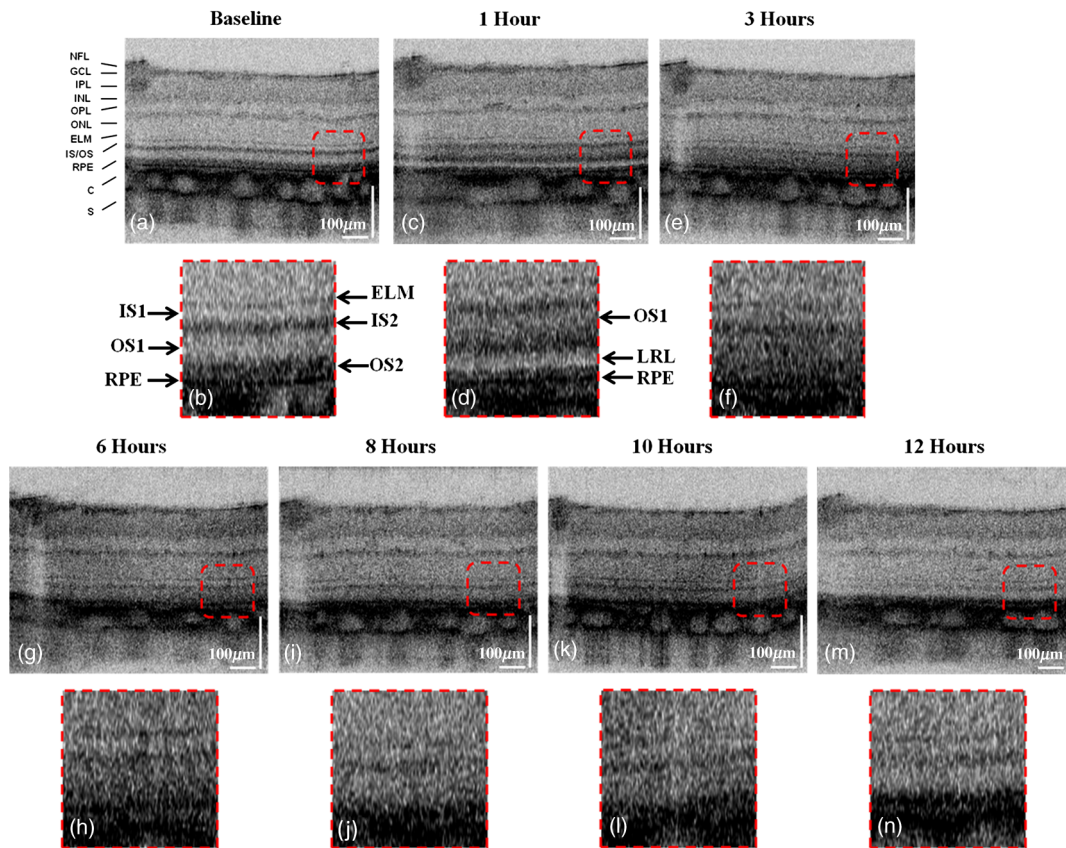


Fig. 2 Representative UHR-OCT cross-sectional images acquired from the same region of the central retina, showing progressive changes in the outer retina due to the toxic effect of the injected drug: baseline (a) and (b) 1 h (c) and (d), 3 h (e) and (f), 6 h (g) and (h), 8 h (i) and (j), 10 h (k) and (l), 12 h (m) and (n). This rat showed the smallest reaction to the drug toxicity among all rats that were not hydrated with PBS.

missing, while the photoreceptor OS layer appears almost homogeneous and highly reflective and can no longer be separated into two distinct bands of low (OS1) and high (OS2) reflectivity, as in the healthy retina. The higher scattering is most likely induced by re-arrangement of the OS, disruption of the membrane disks or both. Six hours post NaIO₃ injection [Fig 2(g) and 2(h)], the reflectivity of the photoreceptor OS layer is somewhat reduced as compared to the previous time point and faint appearance of two bands (OS1 and OS2) is observed, which suggests partial re-arrangement of the OS. This process continues gradually at later time points as observed in Fig. 2(i), 2(j), 2(k), and 2(l), acquired at 8 and 10 h post NaIO₃ injection, respectively. Twelve hours after NaIO₃ injection [Fig. 2(m) and 2(n)], the appearance of the alternating low and highly reflective bands in the IS and OS layers resembles closely the one of the healthy retina [Fig. 2(a) and 2(b)]; however, the overall image contrast of the photoreceptor layer is lower as compared to the baseline image.

The timing of the appearance and disappearance of the LRL and its maximum thickness varied significantly for all rats in the study, as the toxicity of the NaIO₃ drug causes somewhat different systemic reaction in each animal. The results presented in Fig. 2 show an extreme case of the smallest LRL thickness, as well as the earliest and most rapid appearance and disappearance of LRL, that were observed in all animals of this study.

Results presented in Fig. 3 show another extreme case, where the LRL thickness was the largest and the layer disappeared sometime between 10 and 12 h post drug injection. In this

case, the LRL appeared as early as 1 h post NaIO₃ injection [Fig. 3(b)], gradually increased in thickness over the next few hours, reaching a maximum at ~6 to 8 h post drug injection [Fig. 3(e) and 3(f)] and completely disappeared by 12 h [Fig. 3(h)].

Representative results from the histological and immunohistochemical analysis are summarized in Fig. 4. The baseline H&E histological cross-section [Fig. 4(a)] shows the typical normal appearance of the healthy rat retina with clearly defined retinal layers, while the baseline immunohistochemistry image [Fig. 4(f)] shows that the labeling IgG protein remains as expected within the retinal blood vessels, signifying an intact blood-retina barrier (black arrow). One hour post NaIO₃ administration, swelling of the photoreceptor OS is observed in the histological cross-section [Fig. 4(b)]. The toxic photoreceptor damage is even more pronounced in the histology image at 3 h, at which time point, the photoreceptors appear large, friable, and pale due to hydropic change and impaired uptake of the H&E dyes [Fig. 4(c)]. The most drastic morphological change was observed at the sixth-hour time point, when the fluid accumulation causes complete detachment of the photoreceptor OS from the underlying RPE [Fig. 4(d)]. Substantial staining of IgG was detected outside the lumen of inner retinal blood vessels in the immunohistochemistry image acquired at 6 h post NaIO₃ administration [Fig. 4(g)], confirming protein leakage as a consequence of a breakdown of the blood-retinal barrier. The H&E histological cross-section corresponding to 12 h post drug administration [Fig. 4(e)] appears similar to the one acquired at baseline [Fig. 4(a)], except for the swollen and broken RPE cells.

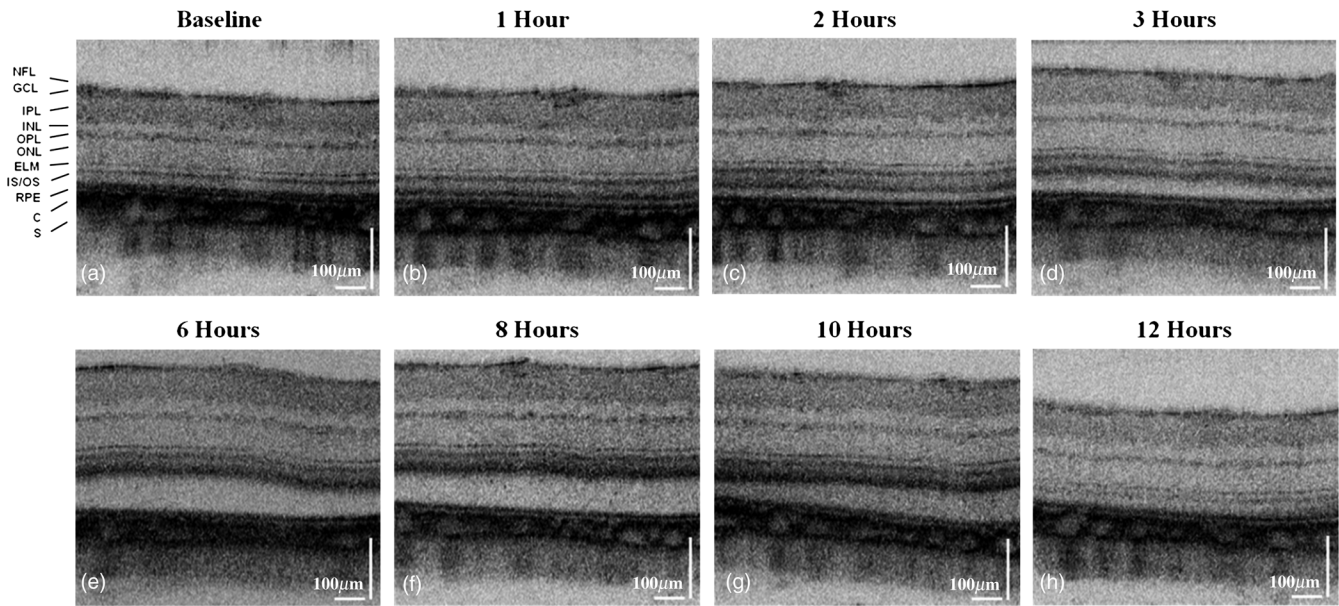


Fig. 3 Representative UHR-OCT cross-sectional images acquired at the same central location of a rat retina depicting the largest reaction to the drug toxicity in the case of no hydration with PBS: baseline (a) and 1 h (b), 2 h (c), 3 h (d), 6 h (e), 8 h (f), 10 h (g), 12 h (h) post NaIO₃ injection.

UHR-OCT and histological images of the NaIO₃ induced damage to the rat outer retina were very similar in terms of morphological changes such as the retinal detachment, the presence of the new LRL and the altered retinal layers thickness and reflectivity, in all imaged animals from both study groups. However, we observed significant difference in the timing of the appearance and disappearance, as well as the maximum thickness of the LRL between animals of the same group and across the two study groups. This difference was much more pronounced for the animals in Group #1, which have not received supplementary subcutaneous PBS

injections, intended to alleviate the systemic effects of the NaIO₃ toxicity.

Volumetric OCT images acquired from all animals in each of the two groups were used for statistical analysis of the retinal layer thickness and optical reflectivity. Quantitative thickness and reflectivity measurements were carried out by segmenting individual retinal layers and the choroid at baseline as well as 3, 8, and 12 h. These time points were selected based on less inter-animal variability. Figure 5 shows a representative UHR-OCT tomogram from a healthy rat retina (baseline measurement) with all retinal layers clearly visible [Fig. 5(a)], along with

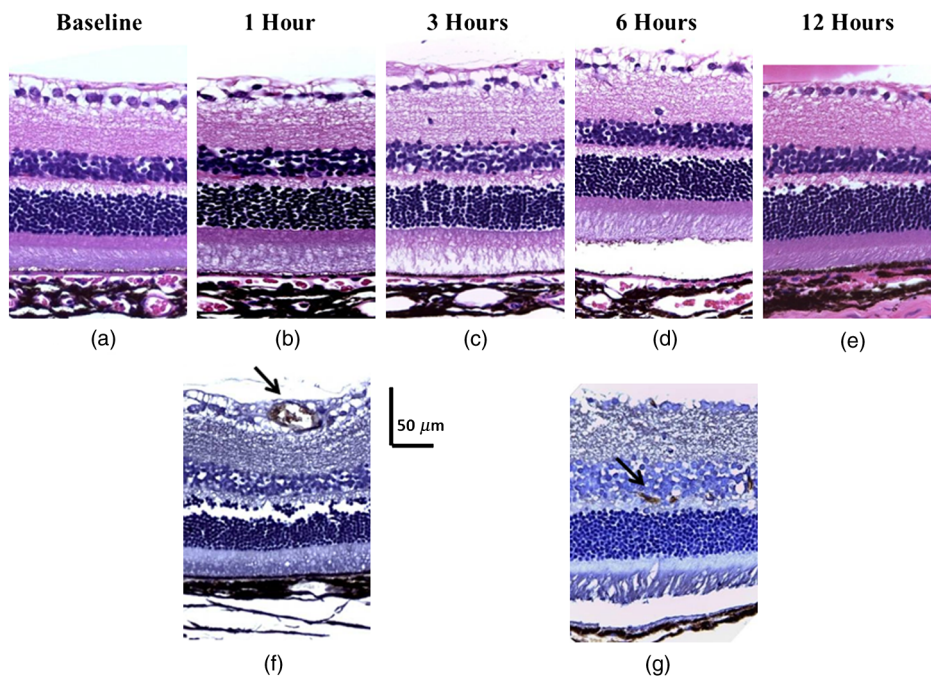


Fig. 4 Representative H&E (a) through (e) and IgG (f) and (g) stained histology images acquired at various time points of the study. Baseline (a) and (f), 1 h (b), 3 h (c), 6 h (d) and 12 h (e) post sodium iodate injection.

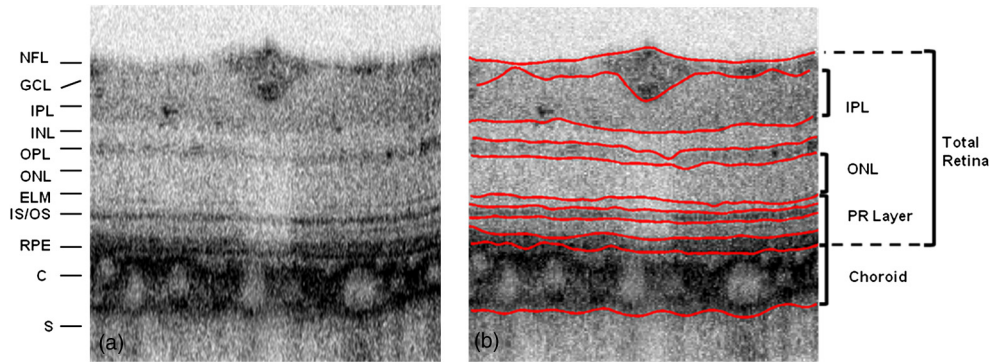


Fig. 5 A representative tomogram of a healthy retina with all layers labeled (a) and segmented (b) Brackets show the regions used for statistical analysis of the data; IPL, ONL, PR Layer, choroid, total retina.

the same image after segmentation with labels indicating the regions used for quantitative statistical analysis [Fig. 5(b)].

Figures 6 and 7 summarize the statistical results for the measure retinal layer thickness and reflectivity. The control group showed no significant difference at any time point compared to the baseline. Therefore, the average (gray solid line) and the standard deviation (gray dotted line) of the values at different time-points acquired from each layer is embedded in the graphs showing data from NaIO₃-injected rats for convenient comparison. Figure 6 shows the variation in the retinal and choroidal thickness as a function of time. The total retinal thickness [Fig. 6(a)] showed significant increase ($p = 0.0000017$) at

3 h after drug injection, which returned to normal value at 8 and 12 h. The choroid [Fig. 6(b)], the IPL [Fig. 6(c)], and the ONL [Fig. 6(d)] showed no statistically significant thickness changes. The thickness of the PR layer (from ELM to RPE) increased significantly ($p = 0.000015$) by 3 h before reducing back to the normal value at later time points as the LRL disappeared [Fig. 6(e)].

Figure 7 shows reflectivity (intensity) changes in the tissue over time within the first 12 h of NaIO₃ injection. The intensity of each layer as well as the total retina and the choroid was normalized to that of the corresponding IPL to compensate for image contrast variability during the different imaging sessions

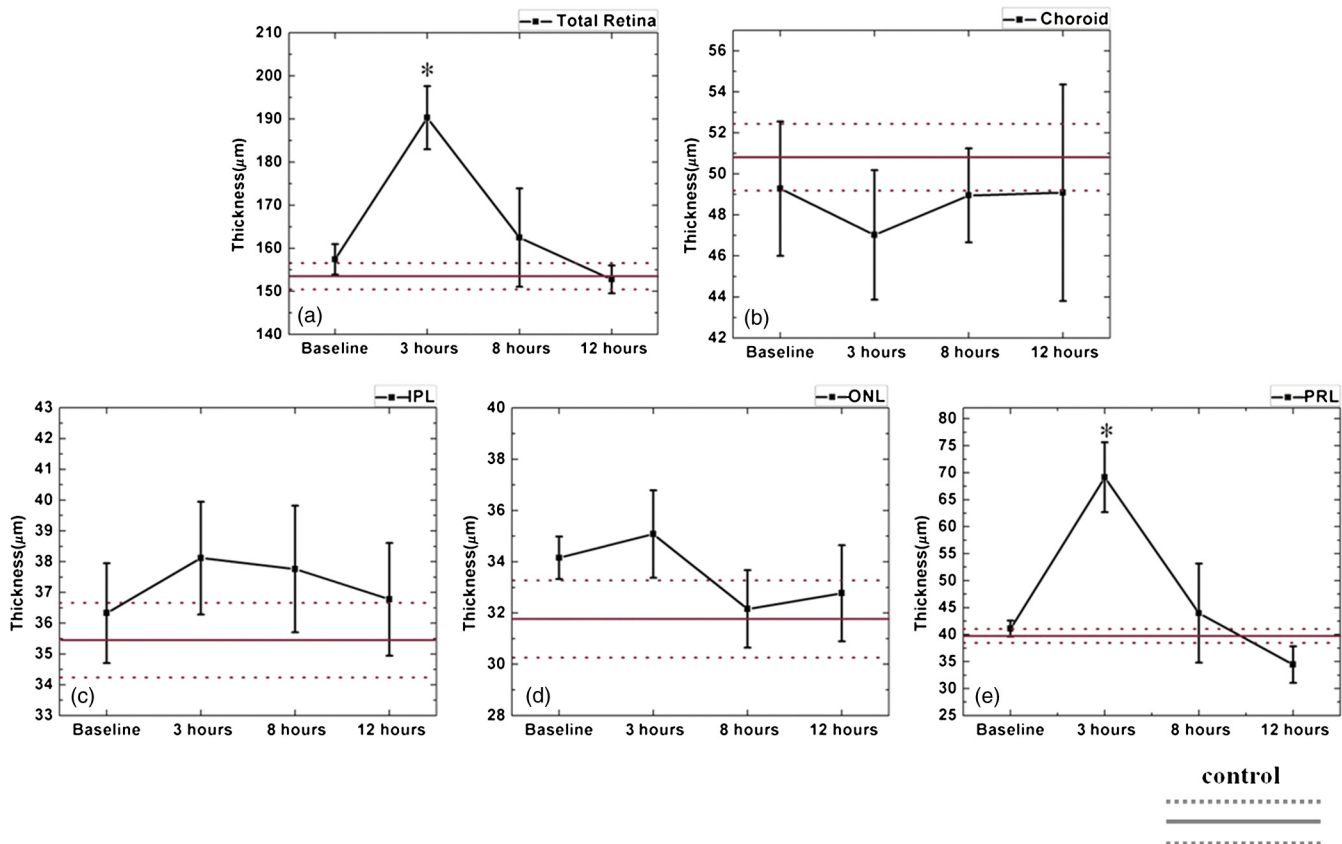


Fig. 6 Statistical analysis of changes in layer thickness at different imaging time points in three sodium iodate treated rats receiving extra 1 mL of subcutaneous PBS injection at 1 and 3 h post drug administration. Graphs represent total retina (a), choroid (b), IPL (c), ONL (d), and PR layer (e) thickness measured at baseline and 3, 8, and 12 h. Mean (gray solid line) and standard deviation (gray dotted line) of the control values acquired from three control rats are presented in each graph.

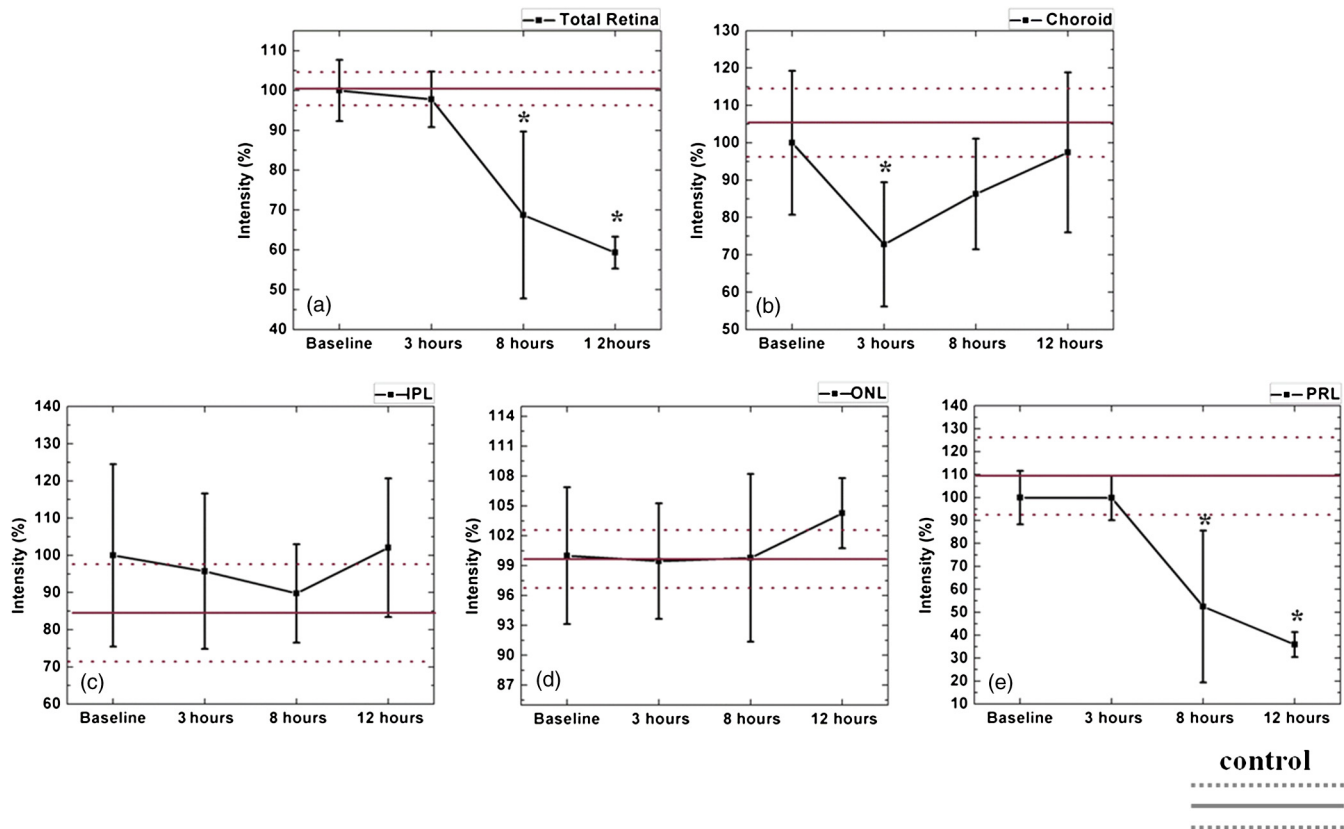


Fig. 7 Statistical analysis of changes in layer reflectivity (intensity) at different imaging time points in three sodium iodate treated rats receiving extra 1 mL of subcutaneous PBS injection at 1 and 3 h post drug administration. Graphs represent total retina (a), choroid (b), IPL (c), ONL (d), and PR layer (e) intensities measured at baseline and 3, 8, and 12 h. Mean (gray solid line) and standard deviation (gray dotted line) of the control values acquired from three control rats are presented in each graph.

due to slight variation in the system performance, light coupling in the animal eye, and possible differences in the image quality in different animals. This normalization was based on the assumption that the IPL remained unaffected by the NaIO₃ induced outer retina degeneration. As reported in previous studies^{3,7,9} and confirmed in our study, the IPL did not change significantly over time [Figs. 6(c) and 7(c)]. The reflectivity values are presented in percentage by setting the baseline value as 100% for convenient comparison. The total retina reflectivity decreased significantly at 8 h ($p = 0.00238$) and remained low ($p = 0.00017$) until 12 h [Fig. 7(a)]. The choroid [Fig. 7(b)], the IPL [Fig. 7(c)], and the ONL [Fig. 7(d)] did not show any significant changes in the reflectivity. The photoreceptor (PR) layer however, showed the highest degree of reflectivity changes. The intensity value dropped significantly at 8 h ($p = 0.00299$; Fig. 7(d)) and remained low until 12 h [$p = 0.00016$; Fig. 7(e)].

4 Discussion

Considering the very low optical reflectivity and dynamics (appearance and disappearance on a time scale of only a few hours) of the LRL, and the clean separation between the photoreceptor OS and the RPE observed in the histological images acquired at 3 and 6 h post injection of NaIO₃, most likely the LRL corresponds to fluid accumulation in the subretinal space. This fluid accumulation may result from the early breakdown of the blood retina barrier and loss of RPE adhesion and active outward transport, as an early response to the NaIO₃

toxicity. This fluid accumulation is followed by changes in the spatial arrangement of the photoreceptor OS, as seen in the histological cross-sections [Fig. 4], as well as changes in the optical reflectivity of the IS and OS layers (Figs. 6 and 7). The spatial rearrangement observed in our study correlates well with disorganization in the photoreceptor OS discs, observed previously with electron microscopy.⁹ We speculate that detachment of the photoreceptor OS from the RPE, and impaired RPE function disrupt the outer segment disc phagocytosis and could lead to disc accumulation of cellular debris, that could explain the local increase of optical scattering. Our statistical analysis shows that the changes in the total retina and PR layer thickness and reflectivity correspond well with the dynamics of the LRL and alterations observed in the PR layer. The PR layer thickness increased by ~68% (~28 μm) 3 h after drug injection [Fig. 6(e)] due to formation of the LRL leading to subsequent ~20% (~33 μm) increase in the total retina thickness [Fig. 6(a)]. As the fluid in the LRL subsides later, the thickness of both PR and total retina decrease and do not show any significant difference from the baseline at 8 and 12 h. Reflectivity changes in the total retina also correspond well with the changes observed in the PR layer. The PR layer intensity [Fig. 7(e)] decreased by ~48% at 8 h post injection due to clearing of the highly reflective material previously observed in the PR space as well as reduced reflectivity of the dark IS2 and OS2 bands. The intensity was decreased further at the last time point (12 h) post NaIO₃ injection by 65% compared with the baseline.

Results from this study also suggest that the early effect of NaIO₃ toxicity on the rat retina varies strongly from animal to animal depending on the animal physiological response to the toxicity of the NaIO₃ drug. The strongest variation in the observed morphological changes in the retina was recorded from Group #1, where the animals were not hydrated with additional subcutaneous PBS injections. These animals also showed severe adverse side effects to the drug toxicity such as blood in the urine. The second group of animals that were hydrated with subcutaneous PBS injections showed less inter-animal variability in the retinal morphological changes and had considerably less adverse side effects to the drug.

5 Conclusions

We have observed and quantified *in vivo* for the first time, the early effect of NaIO₃ on the morphology of the rat outer retina using high speed UHR-OCT. Comparison with histology and immunohistochemistry suggests that changes in the structure and optical reflectivity of the NaIO₃ treated retina correspond to cell swelling, photoreceptor OS rearrangement, and fluid accumulation at the boundary between the OS and the RPE. Our quantitative statistical analysis results suggest that the photoreceptor layer thickness and reflectivity could serve as markers for noninvasive monitoring of outer retinal degeneration. Results from this study could potentially improve our understanding of the mechanisms of outer retina degeneration induced by NaIO₃ and the interplay between the early changes in the photoreceptor morphology and disrupted RPE metabolic and blood-retina barrier function.

Acknowledgments

The authors would like to thank Dr. S. Boyd from St. Michael's hospital, Toronto, and Dr. N. Hutchings from the School of Optometry, University of Waterloo for helpful suggestions related to the NaIO₃ model, H. van der Heide from the University of Waterloo Science Shop for assistance with machining the imaging probe, and N. Gibson from University of Waterloo for assistance with the animal handling. Financial support for this project was provided by the Natural Sciences and Engineering Research Council (NSERC) of Canada.

References

1. A. Machalińska et al., "Sodium iodate selectively injures the posterior pole of the retina in a dose-dependent manner: morphological and electrophysiological study," *Neurochem. Res.* **35**(11), 1819–1827 (2010).
2. K. Kiuchi et al., "Morphologic characteristics of retinal degeneration induced by sodium iodate in mice," *Curr. Eye Res.* **25**(6), 373–379 (2002).
3. L. M. Franco et al., "Decreased visual function after patchy loss of retinal pigment epithelium induced by low-dose sodium iodate," *Invest. Ophthalmol. Vis. Sci.* **50**(8), 4004–4010 (2009).
4. B. Anstadt et al., "Alteration of the blood-retinal barrier by sodium iodate: kinetic vitreous fluorophotometry and horseradish peroxidase tracer studies," *Exp. Eye Res.* **35**(6), 653–662 (1982).
5. W. S. Redfern et al., "Evaluation of a convenient method of assessing rodent visual function in safety pharmacology studies: effects of sodium iodate on visual acuity and retinal morphology in albino and pigmented rats and mice," *J. Pharmacol. Toxicol. Meth.* **63**(1), 102–114 (2011).
6. A. Mizota and E. Adachi-Usami, "Functional recovery of retina after sodium iodate injection in mice," *Vision Res.* **37**(14), 1859–1865 (1997).
7. V. Enzmann et al., "Behavioral and anatomical abnormalities in a sodium iodate-induced model of retinal pigment epithelium degeneration," *Exp. Eye Res.* **82**(3), 441–448 (2006).
8. K. Ohtaka et al., "Protective effect of hepatocyte growth factor against degeneration of the retinal pigment epithelium and photoreceptor in sodium iodate-injected rats," *Curr. Eye Res.* **31**(4), 347–355 (2006).
9. M. Tanaka et al., "Third-order neuronal responses contribute to shaping the negative electroretinogram in sodium iodate-treated rats," *Curr. Eye Res.* **30**(6), 443–453 (2005).
10. G. E. Korte, V. Reppucci, and P. Henkind, "RPE destruction causes choriocapillary atrophy," *Invest. Ophthalmol. Vis. Sci.* **25**(10), 1135–1145 (1984).
11. Y. H. Yoon and M. F. Marmor, "Retinal pigment epithelium adhesion to Bruch's membrane is weakened by hemicholinium-3 and sodium iodate," *Ophthalmic Res.* **25**(6), 386–392 (1993).
12. V. J. Srinivasan et al., "Noninvasive volumetric imaging and morphometry of the rodent retina with high-speed, ultrahigh-resolution optical coherence tomography," *Invest. Ophthalmol. Vis. Sci.* **47**(12), 5522–8 (2006).
13. P. Puvanathan et al., "High-speed, high-resolution Fourier-domain optical coherence tomography system for retinal imaging in the 1060 nm wavelength region," *Opt. Lett.* **33**(21), 2479–2481 (2008).
14. M. Ruggeri et al., "In vivo three-dimensional high-resolution imaging of rodent retina with spectral-domain optical coherence tomography," *Invest. Ophthalmol. Vis. Sci.* **48**(4), 1808–14 (2007).
15. M. V. Sarunic et al., "Longitudinal study of retinal degeneration in a rat using spectral domain optical coherence tomography," *Opt. Express* **18**(22), 23435–41 (2010).
16. M. D. Fischer et al., "In vivo assessment of rodent retinal structure using spectral domain optical coherence tomography," *Adv. Exp. Med. Biol.* **723**, 489–494 (2012).
17. L. R. Ferguson et al., "Modified protocol for *in vivo* imaging of wild-type mouse retina with customized miniature spectral domain optical coherence tomography (SD-OCT) device," *Biol. Proced. Online* **14**(1), 9 (2012).
18. S. Hariri et al., "In vivo assessment of thickness and reflectivity in a rat outer retinal degeneration model with ultrahigh resolution optical coherence tomography," *Invest. Ophthalmol. Vis. Sci.* **53**(4), 1982–1989 (2012).
19. A. Mishra et al., "Intra-retinal layer segmentation in optical coherence tomography images," *Opt. Express* **17**(26), 23719–23728 (2009).
20. R. F. Spaide and C. A. Curcio, "Anatomical correlates to the bands seen in the outer retina by optical coherence tomography: literature review and model," *Retina (Philadelphia, PA.)* **31**(8), 1609–1619 (2011).
21. R. Thar and M. Kühl, "Propagation of electromagnetic radiation in mitochondria," *J. Theor. Biol.* **230**(2), 261–270 (2004).
22. S. Johnsen and E. A. Widder, "The physical basis of transparency in biological tissue: ultrastructure and the minimization of light scattering," *J. Theor. Biol.* **199**(2), 181–198 (1999).
23. A. Brunsting and P. F. Mullaney, "Differential light scattering from spherical mammalian cells," *Biophys. J.* **14**(6), 439–453 (1974).
24. V. V. Tuchin, *Tissue Optics: Light Scattering Methods and Instruments for Medical Diagnosis*, 2nd ed., SPIE Press, Bellingham, WA (2007).